

Adsorption of *para*-Hydrogen on Fullerenes

Joseph D. Turnbull and Massimo Boninsegni

Department of Physics, University of Alberta, Edmonton, Alberta, Canada T6G 2J1

(Dated: November 26, 2018)

Adsorption of *para*-hydrogen on the outer surface of a single fullerene is studied theoretically, by means of ground state Quantum Monte Carlo simulations. We compute energetics and radial density profiles of *para*-hydrogen for various coverages on a variety of small fullerenes. The equilibrium adsorbed solid monolayer is commensurate with the surface of the fullerene; as the chemical potential is increased, a discontinuous change is generally observed, to an incommensurate, compressible layer. Quantum exchanges of hydrogen molecules are absent in these systems.

PACS numbers: 67., 68.08.De, 68.43.-h, 68.60.-p, 68.65.-k, 81.05.Tp

I. INTRODUCTION

Low temperature adsorption of highly quantal fluids, such as helium or *para*-hydrogen (*p*-H₂) on the outer surface of a fullerene (“buckyball”) can provide insight into physical properties of a quantum many-body system confined to spatial regions of nanometer size. As the diameter of the fullerene is increased, the properties of the adsorbate ought to interpolate between those of a cluster with a solvated impurity, and those of an adsorbed film on an infinite substrate.

In this paper, we consider adsorption of *p*-H₂ on a single fullerene C_l, with *l*=20, 36, 60 and 80. All of these molecules are strong adsorbers, and very nearly spherical. Background for this study is provided by the wealth of theoretical^{1,2,3,4,5,6} and experimental^{7,8,9,10,11,12,13} work, spanning over two decades, aimed at investigating the properties of adsorbed *p*-H₂ films on various substrates. This work is also inspired by recent theoretical results on adsorption of helium on buckyballs.^{14,15}

A fluid of *p*-H₂ molecules is an interesting physical system for a number of reasons. Because a *p*-H₂ molecule is half as light as a helium atom, zero-point motion can be expected to be quite significant; each molecule is a spin-zero boson, and therefore it is conceivable that, at low enough temperature, a *p*-H₂ fluid might display physical behavior similar to that of fluid helium, including superfluidity.¹⁶ Unlike helium, though, bulk *p*-H₂ solidifies at low temperature ($T_c \approx 14$ K); this prevents the observation of phenomena such as Bose Condensation and, possibly, superfluidity, which are speculated to occur in the liquid phase below $T \approx 6$ K. Solidification is due to the depth of the attractive well of the potential between two hydrogen molecules, which is significantly greater than that between two helium atoms. Several attempts have been made^{17,18,19,20} to supercool bulk liquid *p*-H₂, but the search for superfluidity (in the bulk) has so far not met with success.

Confinement, and reduction of dimensionality, are widely regarded as plausible avenues to the stabilization of a liquid phase of *p*-H₂ at temperatures sufficiently low that a superfluid transition may be observed. Indeed, computer simulations yielded evidence of superfluid behavior in very small (less than 20 molecules) *p*-H₂ clusters,²¹ and claims have been made of its actual experimental observation.²² Also, a considerable effort has

been devoted, in recent times, to the theoretical characterization of superfluid properties of solvating *p*-H₂ clusters around linear molecules, such as OCS.^{23,24}

The study of hydrogen adsorption on nanocarbons falls within the same general research theme, but is also motivated by possible practical applications; an important example is hydrogen storage, for fueling purposes. So far, research along these lines has mostly focused on nanotubes,^{25,26,27,28,29} but it seems worthwhile to extend the investigation, possibly providing useful quantitative information on adsorption on other nanostructures, including fullerenes.

In this work, energetic and structural properties of a layer of *p*-H₂ molecules adsorbed on a C_l fullerene are investigated theoretically, by means of ground state Quantum Monte Carlo (QMC) simulations. In order to provide a reasonable, quantitative account of the corrugation of the surface of the fullerene, we explicitly modeled in our study each individual carbon (C) atom. For comparison, however, we have also performed calculations with a simpler model, describing fullerenes as smooth spherical surfaces, interacting with *p*-H₂ molecules via an angle-averaged potential.

Only one adsorbed layer is found to be thermodynamically stable on these small nanocarbons. On a corrugated substrate, a commensurate solid layer is observed at equilibrium; as the chemical potential is increased, a discontinuous change to an incommensurate solid layer takes place on C₂₀, C₃₆ and C₆₀. We could not find, within the statistical uncertainties of our calculation, evidence of an incommensurate layer on C₈₀.

The difference in compression between commensurate and incommensurate layers, as measured by the effective *p*-H₂ coverage, is approximately 216% for C₂₀, and decreases to $\sim 25\%$ for C₆₀.

Obviously, on a smooth fullerene, there is no distinction between commensurate and incommensurate layers. In the absence of corrugation, energetics of the adsorbed layer are determined primarily by the interactions among *p*-H₂ molecules. The ground state of *p*-H₂ in two dimensions (2D) is a solid, with molecules forming a triangular lattice.^{3,30} Our results indicate that *p*-H₂ molecules attempt to reproduce the same triangular arrangement as on an infinite plane, even when confined to moving on a spherical surface of radius as small as a few Å.

Evidence of quantum exchange is absent in these sys-

tems, i.e., no evidence suggesting possible superfluid behavior is gathered in this work.

The remainder of this manuscript is organized as follows: Sec. II offers a description of the model used for our system of interest, including a discussion of the potentials used and the justifications for underlying assumptions. Sec. III involves a brief discussion of the computational technique and specific details of its implementation, in addition to details of calibration and optimization. The results are presented in Sec. IV; finally, Sec. V is a summary of the findings and our concluding remarks.

II. MODEL

We consider a system of N p -H₂ molecules, in the presence of a single C_l molecule. The latter is assumed fixed in space, owing to its relatively large mass; the center of the molecule is taken as the origin of a Cartesian coordinate frame. The l individual C atoms are fixed at positions $\{\mathbf{R}_k\}$, $k=1,2,\dots,l$. All of the atoms and molecules are regarded as point particles. The model quantum many-body Hamiltonian is therefore the following:

$$\hat{H} = -\frac{\hbar^2}{2m} \sum_{i=1}^N \nabla_i^2 + \sum_{i<j} V(r_{ij}) + \sum_{i=1}^N \sum_{k=1}^l U(|\mathbf{r}_i - \mathbf{R}_k|) \quad (1)$$

Here, m is the mass of a p -H₂ molecule, $r_{ij} \equiv |\mathbf{r}_i - \mathbf{r}_j|$, $\{\mathbf{r}_j\}$ (with $j=1,2,\dots,N$) are the positions of the p -H₂ molecules, V is the potential describing the interaction between any two of them, and U represents the interaction of a p -H₂ molecule with a C atom. All pair potentials are assumed to depend only on relative distances. The interaction V is described by the Silvera-Goldman potential³¹, which provides an accurate description of energetic and structural properties of condensed p -H₂ at ordinary conditions of temperature and pressure.^{32,33} The interaction of a p -H₂ molecule and a C atom is modeled using a standard 6-12 Lennard-Jones (LJ) potential, with $\epsilon = 32.05$ K and $\sigma = 3.179$ Å (see, for instance, Ref. 29).

The model (1) already contains important physical simplifications, such as the neglect of zero-point motion of C atoms, as well as the restrictions to additive pairwise interactions (to the exclusion of, for example, three-body terms), all taken to be central, and the use of the highly simplified LJ interaction. On the other hand, (1) is the simplest microscopic model that explicitly takes into account the corrugation of the surface of the buckyball.

A further simplification can be introduced by replacing the third term in (1) with $\sum_i \tilde{U}(r_i)$, where \tilde{U} is the following, spherically symmetric external potential (see Ref. 14 for details):

$$\tilde{U}(r, R) = \frac{\epsilon n}{Rr} \left\{ \frac{\sigma^{12}}{5} \left[\frac{1}{(r-R)^{10}} - \frac{1}{(r+R)^{10}} \right] - \frac{\sigma^6}{2} \left[\frac{1}{(r-R)^4} - \frac{1}{(r+R)^4} \right] \right\} \quad (2)$$

Here, $n = 4\pi\theta a^2$, a being the of the fullerene and θ being the areal density of C atom on its surface; ϵ and σ are the parameters of the LJ potential V introduced for the fully corrugated model. By using (2), one is describing the fullerene as a smooth spherical shell, i.e., corrugation is neglected. This approximation substantially simplifies the calculation; it has been adopted in recent studies of helium adsorption on buckyballs.^{14,15} As mentioned above, in this work we have performed calculations based on the full model (1), as well as using the effective potential (2); results obtained in the two ways are compared in Sec. IV.

III. COMPUTATIONAL METHOD

Accurate ground state expectation values for quantum many-body systems described by a Hamiltonian such as (1) can be computed by means of QMC simulations. In this work, the method utilized is *Variational Path Integral* (VPI), which is an extension to zero temperature of the standard, Path Integral Monte Carlo (PIMC) method.³⁶ VPI (also referred to as Path Integral Ground State, PIGS³⁷) is a projection technique, which filters out the exact ground state wave function out of an initial trial state. It is therefore closely related to other ground state projection methods, such as Diffusion Monte Carlo (DMC), but has a few distinct advantages (for a discussion, see, for instance, Ref. 37).

The VPI technique works as follows: One samples a large set $\{X^m\}$, $m = 1, 2, \dots, M$, of discretized many-particle paths $X \equiv R_0 R_1 \dots R_{2L}$, where $R_j \equiv \mathbf{r}_{j1} \mathbf{r}_{j2} \dots \mathbf{r}_{jN}$ represents the positions of all N particles in the system at the j th ‘‘slice’’. These paths are sampled based on the probability density

$$\mathcal{P}(X) \propto \Psi_T(R_0) \Psi_T(R_{2L}) \left\{ \prod_{j=0}^{2L-1} G(R_j, R_{j+1}, \tau) \right\} \quad (3)$$

where $\Psi_T(R)$ is a trial wave function for the many-body system, and $G(R, R', \tau)$ is a short-time (i.e., $\tau \rightarrow 0$) approximation to the imaginary-time propagator $\langle R | \exp[-\tau \hat{H}] | R' \rangle$. One can show³⁶ that, for any choice of Ψ_T , in the limits $L\tau \rightarrow \infty$, $\tau \rightarrow 0$, R_L is sampled from the square of the exact ground state wave function $\Phi(R)$. This allows one to calculate the ground state expectation value of any observable \hat{O} diagonal in the coordinate representation as a simple statistical average

$$\langle \hat{O} \rangle \approx \frac{1}{M} \sum_{m=1}^M \mathcal{O}(R_L^m) \quad (4)$$

The ground state energy can be evaluated using the convenient ‘‘mixed estimator’’, which yields an unbiased estimate:

$$\langle \hat{H} \rangle \approx \sum_{m=1}^M \frac{\hat{H} \Psi_T(R_1^m)}{\Psi_T(R_1^m)} \quad (5)$$

Both expressions (4), (5) can be rendered arbitrarily accurate by letting $M \rightarrow \infty$.

The form of G used here is the *primitive approximation*

$$G(R, R', \tau) = \rho_F(R, R', \tau) e^{-\frac{\tau}{2}[\bar{U}(R) + \bar{U}(R')]} + O(\tau^3), \quad (6)$$

where $\bar{U}(R)$ is the total potential energy of the system at the configuration R , and

$$\rho_F(R, R', \tau) = (4\pi\lambda\tau)^{-3N/2} \prod_{i=1}^N \exp\left[-\frac{(\mathbf{r}_i - \mathbf{r}'_i)^2}{4\lambda\tau}\right] \quad (7)$$

is the exact propagator for a system of N non-interacting particles.

For a particular choice of τ , since the projection time $\lambda = L\tau$ is necessarily finite, simulations must be performed for increasing L , until one finds that estimates of the observables have converged, within statistical errors. One must also extrapolate estimates obtained for different τ , in order to infer results in the $\tau \rightarrow 0$ limit. A more accurate form of G (such as that thoroughly discussed in Ref. 39, accurate to τ^4), or a more accurate trial wave function Ψ_T allows one to obtain convergence with larger τ and/or shorter L , but, at least in principle, the extrapolated results ought to be independent of the choices of G and Ψ_T .⁴³ In summary, with sufficient computer time and proper calibration of τ and L , one can generate estimates of physical observables that are *exact* (errors being only statistical).

Individual simulations involve generating the set $\{X^m\}$ using a random walk through path space. The same path sampling techniques of PIMC are adopted; included are trial moves involving rigid displacements of an entire particle path (*displace* type moves), and multilevel sampling updates (see, for instance, Ref. 36), which are divided into moves of central path portions (i.e., not including an endpoint, namely $j=1$ or $j=2L$), and moves that update endpoint configurations (which involve Ψ_T in the acceptance test, as do the *displace* moves).

The trial wave function utilized is of the Jastrow type:

$$\Psi_T(\mathbf{r}_1, \mathbf{r}_2, \dots, \mathbf{r}_N) = \left(\prod_{i=1}^N \prod_{k=1}^l e^{-w(|\mathbf{r}_i - \mathbf{R}_k|)} \right) \times \left(\prod_{i < j}^N e^{-u(r_{ij})} \right) \quad (8)$$

which fulfills the symmetry requirement of a many-boson wave function. In the case of the spherically averaged model, $l=1$ and $R_1=0$. The pseudo-potentials w and u were chosen as follows:

$$w(r) = \frac{\alpha}{r^x} \quad \text{and} \quad u(r) = \frac{\gamma}{r^5} \quad (9)$$

where $x = 2$ for the spherically averaged potential, and $x = 5$ for the corrugated case. The values of the parameters $\alpha = 80 \text{ \AA}^x$, $\gamma = 750 \text{ \AA}^5$ and x were obtained empirically, by minimizing the energy expectation value computed in separate variational calculations.

Using the given Ψ_T , we observe convergence of the ground state energy estimates with a projection time $L\tau = 0.250 \text{ K}^{-1}$, with $\tau = \tau_o = 1/640 \text{ K}^{-1}$. Estimates for all quantities quoted in this study were obtained using $\tau = \tau_o$, even though convergence of the estimates for structural quantities can be typically observed with values of τ significantly greater than τ_o (for an equal projection time).

VPI calculations for a range of $p\text{-H}_2$ coverages were carried out for each of C_{20} , C_{36} , C_{60} , and C_{80} (we refer here to the near spherical isomers of each). We use an initial configuration of para-hydrogen molecules surrounding the fullerene at a distance of approximately twice the C_l radius (i.e., making sure that no $p\text{-H}_2$ start off within the buckyball). Because of the strongly attractive character of the C_l , for a small enough number of surrounding hydrogen molecules the system remains spatially confined (i.e., $p\text{-H}_2$ molecules do not evaporate). Thus, even though periodic boundary conditions are used in the simulation, they have no effect, so long as a sufficiently large simulation cell is used.

The systematic errors of our calculation are attributable to the finite projection time $L\tau$ and the finite time step τ . Based on comparisons of results obtained from simulations with different values of L and τ , we estimate our combined systematic error on the total energy per $p\text{-H}_2$ molecule to be of the order of 0.6 K or less.

IV. RESULTS

Physical quantities of interest include the ground state energy per $p\text{-H}_2$ molecule $e(N)$ and the radial $p\text{-H}_2$ density $\rho(r)$ about the fullerene, as a function of the total number N of molecules. Results for $e(N)$ for all fullerenes considered in this study are shown in Figs. 1 through 4.

Let us consider first the case of C_{20} (shown in Fig. 1), as it allows us to illustrate some of the general features seen on other fullerenes as well. Filled circles represent the energy estimates yielded by the fully corrugated model (1), whereas filled squares represent estimates obtained using the spherically averaged potential \tilde{U} described in Sec. II. Solid lines are polynomial fits to the numerical data. Also shown in the inset is the number of adsorbed molecules N versus the chemical potential μ (in K). This is obtained by first fitting the results for $e(N)$, then minimizing the grand canonical potential $\phi(N) = N(e(N) - \mu)$ with respect to N , for different values of μ . The chemical potential of bulk solid $p\text{-H}_2$ at zero temperature, computed by Quantum Monte Carlo using the Silvera-Goldman potential, is $\mu_o = -88 \text{ K}$ (from Ref. 33), and that is where all of the $N(\mu)$ curves end.

There are some qualitative similarities, but also important differences (mainly at low N) between the results yielded by the two models utilized. Firstly, in the large- N limit they yield essentially the same energy estimates, as corrugation becomes unimportant for thick adsorbed films. This is the case on all fullerenes.

Both $e(N)$ curves display a single minimum at a specific number \tilde{N} of $p\text{-H}_2$ molecules. The minimum cor-

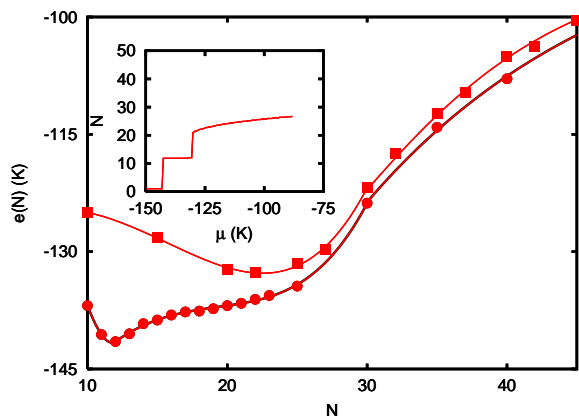


FIG. 1: (Color online) Energy per p -H₂ molecule $e(N)$ computed by VPI, as a function of the number of molecules adsorbed on a C₂₀ fullerene. Filled squares: results obtained with the angularly averaged potential (2). Filled circles: results obtained by explicitly modeling all carbon atoms in the fullerene. Solid lines are polynomial fits to the VPI data. Inset shows the number of particles N plotted as a function of the chemical potential μ , for the fully corrugated model. The chemical potential of bulk solid p -H₂ is -88 K (from Ref. 33), and that is where the $N(\mu)$ curve ends.

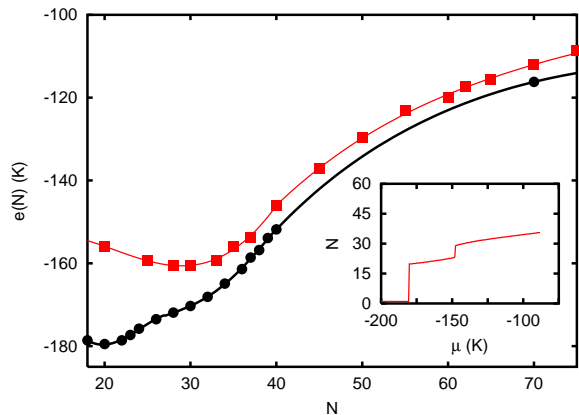


FIG. 2: (Color online) Same as Fig. 1, but for a C₃₆ fullerene. The commensurate layer has $N_C = 20$ p -H₂ molecules and is compressible, as evidenced by the finite slope of the curve $N(\mu)$ for $20 \leq N \leq 28$.

responds to the mathematical condition $e(\bar{N}) = \mu(\bar{N})$, and physically to the formation of a stable p -H₂ layer. On the corrugated C₂₀, a stable layer occurs for a number $\bar{N} \equiv N_C = 12$, significantly smaller than that ($\bar{N} \equiv N_S = 22$) obtained on a smooth fullerene. Moreover, the energy per molecule $e_C(\bar{N}_C)$ for the corrugated model, is approximately 10% lower than that on a smooth substrate ($e_S(\bar{N}_S)$), i.e., the corrugated model yields stronger p -H₂ binding. Qualitatively similar results are observed on all fullerenes; however, the difference between N_C and N_S is seen to decrease with the radius of the fullerene, whereas the difference between the minimum energy values in the two models is $\sim 10\%$ for all fullerenes.

Corrugation introduces the conceptual distinction be-

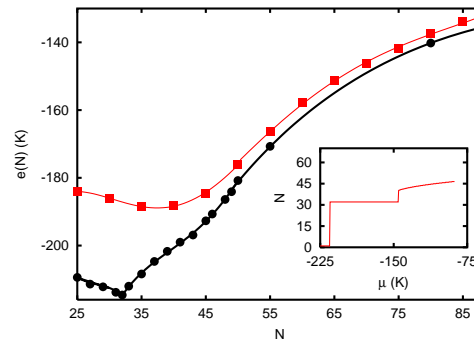


FIG. 3: (Color online) Same as Fig. 1, but for a C₆₀ fullerene.

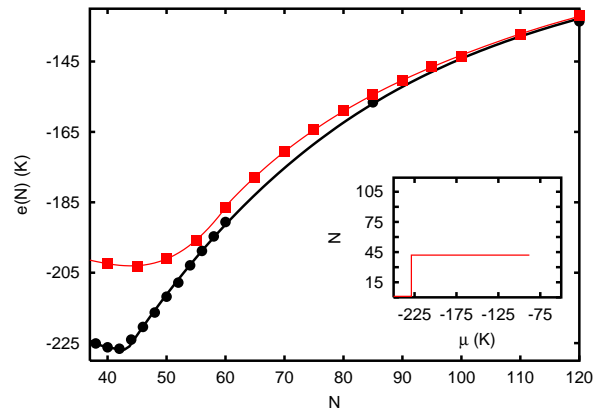


FIG. 4: Same as Fig. 1, but for a C₈₀ fullerene.

tween a layer that is *commensurate* with the substrate (i.e., the outer surface of the fullerene), and one that is *incommensurate* with it. In a commensurate layer, each p -H₂ molecule sits right on top of the center of one of the hexagonal (or, pentagonal) faces of the polyhedron formed by C atoms. For example, C₂₀ has the shape of a dodecahedron, i.e. it has 12 pentagonal faces, corresponding to as many adsorption sites for p -H₂ molecules. In an incommensurate layer, on the other hand, the arrangement of p -H₂ molecules is mostly determined by their mutual interactions; the fullerene, in this case, merely provides a background attractive potential and a curved geometry.

On all fullerenes studied here, using the corrugated model, the equilibrium adsorbed p -H₂ layer is found to be commensurate. On a corrugated substrate, one normally sees a transition from a commensurate to an incommensurate layer, as the chemical potential is increased from its equilibrium value.⁴ No such transition can be observed on a smooth substrate, for which commensuration is undefined. This is indeed what we *generally* observe on the various fullerenes that we have considered. Details, however, differ for the different systems.

On C₂₀, the number of adsorbed p -H₂ molecules remains constant as the chemical potential is increased (i.e., no compression of the commensurate layer is observed), until it jumps discontinuously from $N_C = 12$ to $N_I = 22$ (see Fig. 1). This signals the (abrupt) appearance of

C_l	a	N_C	θ_C	N_I	θ_I	N_S	θ_S
C_{20}	2.00	12	0.2387	22	0.4377	22	0.4377
C_{36}	2.75	20	0.2105	28	0.2946	30	0.3157
C_{60}	3.55	32	0.2021	40	0.2526	40	0.2526
C_{80}	4.11	42	0.1979	-	-	45	0.2120

TABLE I: Effective p -H₂ monolayer coverages for both the corrugated and uncorrugated models of the fullerenes. For the model including corrugation, N_C and N_I mark the number of p -H₂ molecules in the adsorbed layer at commensuration and incommensuration, respectively, with coverages θ_C and θ_I (in \AA^{-2}). The number N_S marks the number of p -H₂ molecules in the adsorbed layer on a smooth fullerene, θ_S being the corresponding coverage. The radius a of each fullerene (in \AA) is also given.

an incommensurate layer. The number N_I of molecules in such an incommensurate layer is the same as in the equilibrium layer on a smooth C_{20} ; this leads us to surmise that the physics of the incommensurate layer on the corrugated fullerene and that of the equilibrium layer on the smooth fullerene are essentially the same. Thus, the main effect of the neglect of corrugation associated with the spherically averaged potential model, is the absence of the commensurate layer. We come back to this point later, when discussing density profiles.

The incommensurate layer that forms on a C_{20} fullerene is compressible, i.e., the number of adsorbed molecules is seen to increase monotonically with μ , up to $N \sim 28$; no second layer formation is seen before μ reaches the value (μ_o) corresponding bulk p -H₂, above which thicker adsorbed films are thermodynamically unstable. In fact, on none of the fullerenes considered here, do we find more than one stable adsorbed layer.

On C_{36} , our results indicate that the commensurate layer is compressible; here too, however, a discontinuous transition occurs to an incommensurate layer, also compressible and again physically similar to the one that forms on a smooth fullerene.

The same physical behavior to that observed on C_{20} is seen on C_{60} and C_{80} , with an incompressible commensurate layer. On C_{80} , though, we fail to observe an incommensurate layer; it should also be noticed that, on this system, it is $N_C = 42$ and $N_S = 45$, i.e., there is a much smaller relative difference between N_C and N_S than on the other fullerenes. Our results are summarized in Table I, where the numbers are listed of p -H₂ molecules N_C and N_I in the commensurate and incommensurate layers adsorbed on a corrugated fullerene, as well as N_S for a smooth fullerene. Also shown are the values of the effective coverage (2D density)

$$\theta = \frac{N}{4\pi R^2} \quad (10)$$

where, again, a is the radius of the fullerene. The effect of the curvature of the substrate can be quantitatively established by comparing these values of θ to the equilibrium coverage of p -H₂ on a graphite substrate,⁴ estimated at 0.070 \AA^{-2} . It should be noted that this definition of θ is used to compare the coverage as a function of the

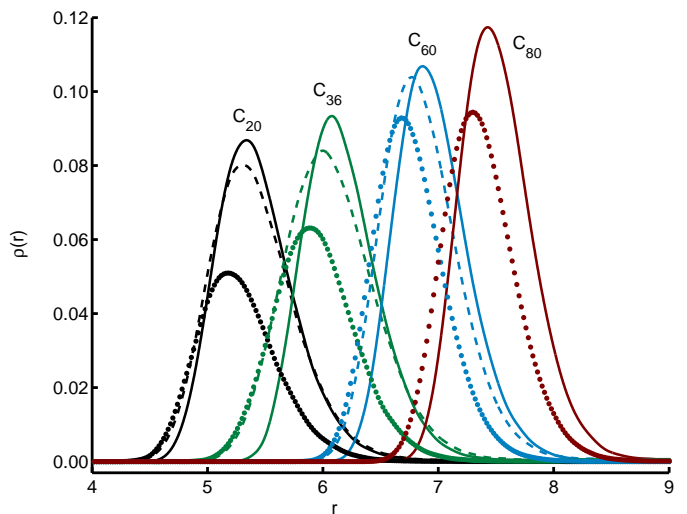


FIG. 5: (Color online) Radial density profiles of a p -H₂ layer adsorbed on C_l . Solid lines: profiles obtained for the smooth fullerene model. Dotted lines: profiles of commensurate layers on corrugated model. Dashed lines: profiles of incommensurate layers on corrugated models. Density is given in \AA^{-3} , whereas the distance r from the center of the fullerene is given in \AA .

surface area of the substrate. A definition of the coverage incorporating the distance at which the p -H₂ sit above the fullerenes is given below (the two definitions would be equivalent for a planar substrate, a distinction only arising with the introduction of non-zero curvature).

Structural information about these systems is offered by the radial density profiles $\rho(r)$ of p -H₂ on each of the four C_l for the two models, all shown in Fig. 5. Solid lines denote the radial profiles on a smooth fullerene, while dotted and dashed lines denote radial density profiles in the corrugated model at commensuration and incommensuration, respectively. These results are qualitatively the same for each fullerene. The peak of the profile is shifted away from the center of the fullerene, as the system makes a transition from a commensurate to an incommensurate layer, which is not physically unexpected. No evidence is seen of second layer formation, on any of the fullerenes studied here, for values of the chemical potential for which the adsorbed film is thermodynamically stable (i.e., $\mu \leq \mu_o$).

On comparing the density profile for the incommensurate layer on a corrugated fullerene (dashed lines) with that for a smooth fullerene (solid lines), one observes a further shift to the right for the case of a spherically averaged potential. Perhaps more interestingly, the incommensurate layer on a corrugated fullerene features a greater spatial width, with respect to that on a smooth fullerene (particularly on C_{20} and C_{36}). Otherwise, these layers seem physically similar; for example, one can compute an effective 2D density θ_{eff} (different than the coverage θ discussed above) defined as

$$\theta_{eff} = \frac{N}{4\pi a_p^2} \quad (11)$$

where a_p is the position of the peak of $\rho(r)$. The values obtained for the two layers are very close. In the case of a smooth fullerene, as one goes from C_{20} to C_{80} , θ_{eff} approaches from below the value 0.067 \AA^{-2} , namely the equilibrium density of $p\text{-H}_2$ in 2D.³⁰ This suggests that the physics of the incommensurate layer (and that on a smooth fullerene) is determined primarily by the interaction among $p\text{-H}_2$ molecules, which attempt to replicate, on a curved surface, the same arrangement as in 2D. One further thing to note is that the width of the adsorbed $p\text{-H}_2$ layer on these systems is of the order of 1 \AA , very close to that of an adsorbed monolayer film on graphite.⁴

The computational method adopted here does not allow one to make a direct estimation of the $p\text{-H}_2$ molecule exchange frequency, unlike its finite temperature counterpart (Path Integral Monte Carlo). Nevertheless, from visual inspection of many-particle configurations generated in the Monte Carlo simulation, we observe little or no overlap of paths associated to different molecules, which is substantial evidence that many-particle permutations are absent in this system. This is consistent with the high degree of localization that molecules experience, both in the commensurate and in the incommensurate adsorbed layers.

V. CONCLUSIONS

Using a numerically exact ground state Quantum Monte Carlo method, we studied $p\text{-H}_2$ adsorption on the outer surface of near-spherical fullerenes. We performed calculations based on a simple model, in which all carbon atoms are included explicitly, i.e., corrugation of the surface of the fullerene is captured.

A single solid layer of $p\text{-H}_2$ is found to be thermodynamically stable on the fullerenes studied in this work. We find that the equilibrium adsorbed layer is commensurate with the corrugated surface of the fullerene. Such a layer is found to be compressible on one of the fullerenes (namely, C_{36}), incompressible on the others. On increasing the chemical potential, a discontinuous transition is observed to an incommensurate layer on all fullerenes,

except for the largest one considered here (C_{80}).

The basic physics of the incommensurate layer is driven primarily by the interaction among $p\text{-H}_2$ molecules, which attempt to reproduce the same triangular arrangement as on an infinite plane, even when confined to moving on a spherical surface of radius as small as a few \AA . Indeed, the incommensurate layer is very similar to that found using a simpler model of the system, describing the fullerene as a smooth spherical substrate. This simpler model yields results for the energetics and structure of the incommensurate layer in good quantitative agreement with those provided by the fully corrugated model; obviously, however, it is necessary to include corrugation in order to reproduce the commensurate layer. An interesting question that arises is whether a commensurate layer of helium may exist on these molecules; the theoretical studies performed so far have made use of a spherically averaged potential to describe the fullerenes.¹⁴

No evidence of quantum exchanges among $p\text{-H}_2$ molecules has been observed in this work. Thus, these systems do not appear as not likely candidates for the observation of the elusive superfluid phase of *para*-hydrogen.

In conclusion, this study has provided preliminary information on the structure and energetics of hydrogen films adsorbed to the exterior of buckyballs, though much remains to be answered. The experimental tests of several of the stated predictions could be carried out, for example, by measuring the mass of adsorbed hydrogen on C_l by examination of excitation spectra in a dipole trap.^{40,41,42}

Acknowledgments

This work was supported in part by the Petroleum Research Fund of the American Chemical Society under research grant 36658-AC5, by the Natural Sciences and Engineering Research Council of Canada (NSERC) under research grant G121210893, and by an NSERC PGSA scholarship.

¹ M. Wagner and D. M. Ceperley, *J. Low Temp. Phys.* **94**, 161 (1994).

² M. Wagner and D. M. Ceperley, *J. Low Temp. Phys.* **102**, 275 (1996).

³ M. C. Gordillo and D. M. Ceperley, *Phys. Rev. Lett.* **79**, 3010 (1997).

⁴ K. Nho and E. Manousakis, *Phys. Rev. B*, **65**, 115409 (2002).

⁵ W. Shi, J. K. Johnson and M. W. Cole, *Phys. Rev. B* **68**, 125401 (2003).

⁶ M. Boninsegni, *Phys. Rev. B* **70**, 125405 (2004).

⁷ M. Nielsen, J. P. McTague and L. Passell in *Phase Transitions in Surface Films*, edited by J. Dash and J. Ruvalds (Plenum, New York, 1980).

⁸ H. J. Lauter, H. Godfrin, V. L. P. Frank and P. Leiderer in *Phase Transitions in Surface Films 2*, edited by H. Taub,

G. Torzo, H. J. Lauter and S. C. Fain Jr. (Plenum, New York, 1990).

⁹ H. Wiechert in *Excitations in Two-Dimensional and Three-Dimensional Quantum Fluids*, edited by A. F. G. Wyatt and H. J. Lauter (Plenum, New York, 1991).

¹⁰ F. C. Liu, Y. M. Liu and O. E. Vilches, *J. Low Temp. Phys.* **89**, 649 (1992).

¹¹ E. Cheng, G. Mistura, H. C. Lee, M. H. W. Chan, M. W. Cole, C. Carraro, W. F. Saam and F. Toigo, *Phys. Rev. Lett.* **70**, 1854 (1993).

¹² G. Mistura, H. C. Lee and M. H. W. Chan, *J. Low Temp. Phys.* **96**, 221 (1994)

¹³ D. Ross, P. Taborek and J. E. Rutledge, *Phys. Rev. B* **58**, R4274 (1998).

¹⁴ E. S. Hernandez, M. W. Cole, and M. Boninsegni, *Phys. Rev. B* **68** 125418 (2003).

- ¹⁵ L. Szybisz and I. Urrutia, *J. Low Temp. Phys.* **134**, 516 (2004).
- ¹⁶ V. L. Ginzburg and A. A. Sobyenin, *JETP Letters* **15**, 242 (1972).
- ¹⁷ M. Bretz and A. L. Thomson, *Phys. Rev. B* **24**, 467 (1981).
- ¹⁸ G. M. Seidel, H. J. Maris, F. I. B. Williams and J. G. Cardon, *Phys. Rev. Lett.* **56**, 2380 (1986).
- ¹⁹ H. J. Maris, G. M. Seidel and F. I. B. Williams, *Phys. Rev. B* **36**, 6799 (1987).
- ²⁰ M. Schindler, A. Dertinger, Y. Kondo and F. Pobell, *Phys. Rev. B* **53**, 11451 (1996).
- ²¹ P. Sindzingre, D. M. Ceperley and M. L. Klein, *Phys. Rev. Lett.* **67**, 1871 (1991).
- ²² S. Grebenev, B. Sartakov, J. P. Toennies and A. F. Vilesov, *Science* **289**, 1532 (2000).
- ²³ Y. Kwon and K. B. Whaley, *Phys. Rev. Lett.* **89**, 273401 (2002).
- ²⁴ F. Paesani, R. F. Zillich and K. B. Whaley, *J. Chem. Phys.* **119**, 11682 (2003).
- ²⁵ A. C. Dillon, K. M. Jones, T. A. Bekkedahl, C. H. Kiang, D. S. Bethune and M. J. Heben, *Nature (London)* **386**, 377 (1997).
- ²⁶ C. Liu, Y. Y. Fan, M. Liu, H. T. Cong, H. M. Cheng and M. S. Dresselhaus, *Science* **286**, 1127 (1999).
- ²⁷ Q. Wang and J. K. Johnson, *J. Chem. Phys.* **110**, 577 (1999).
- ²⁸ B. K. Pradhan, A. R. Harutyunyan, D. Stojkovic, J. C. Grossman, P. Zhang, M. W. Cole, V. H. Crespi, H. Goto, J. Fujiwara, and P. C. Eklund, *J. Mater. Res.* **17**, 2209 (2002).
- ²⁹ D. Levesque, A. Gicquel, F. L. Darkrim, and S. B. Kayiran, *J. Phys. CM* **14**, 9285 (2002).
- ³⁰ M. Boninsegni, *Phys. Rev. B* **70**, 193411 (2004).
- ³¹ I.F. Silvera and V.V. Goldman, *J. Chem. Phys.* **69**, 4209 (1978).
- ³² Q. Wang, J. K. Johnson and J. Q. Broughton, *Mol. Phys.* **89**, 1105 (1996).
- ³³ F. Operetto and F. Pederiva, *Phys. Rev. B* **69**, 024203 (2004).
- ³⁴ M. Pierce and E. Manousakis, *Phys. Rev. B* **59**, 3802 (1999).
- ³⁵ X. Z. Ni and L.W. Bruch, *Phys. Rev. B* **33**, 4584 (1986).
- ³⁶ D.M. Ceperley, *Rev. Mod. Phys.* **67**, 279 (1995).
- ³⁷ A. Sarsa, K. E. Schmidt and W. R. Magro, *J. Chem. Phys.* **113**, 1366 (2000).
- ³⁸ L. W. Bruch, M. W. Cole, and E. Zaremba, *Physical Adsorption* (Oxford UP, Oxford, 1997).
- ³⁹ S. Jang, S. Jang and G. A. Voth, *J. Chem. Phys.* **115**, 7832 (2001).
- ⁴⁰ D.J. Han, S. Wolf, S.J. Oliver, C. McCormick, M.T. DePue, and D.S. Weiss, *Phys. Rev. Lett.* **85**, 724 (2000).
- ⁴¹ M.E. Gehm, K.M. O'Hara, T.A. Savard, and J.E. Thomas, *Phys. Rev. A* **61**, 029902 (2000).
- ⁴² E. Riis and S.M. Barnett, *Europhys. Lett.* **21**, 533 (1993); **30**, 441 (1995).
- ⁴³ Strictly speaking, there is an additional requirement, namely that Ψ_T not be orthogonal to the true ground state wave function. This is not a problem for Bose systems, since the ground state wave function can always be chosen real and positive, and therefore any positive-definite function Ψ_T satisfies the non-orthogonality requirement.